Effects of Ar^+ etching of $Cu_2ZnSnSe_4$ thin films: a X-Ray Photoelectron Spectroscopy and Photoluminescence study

M.V. Yakushev,[1,2,3,4] M.A. Sulimov,[2,3] E. Skidchenko,[5,1] J. Márquez-Prieto,[6] I. Forbes,[6] P.R. Edwards,[1] M.V. Kuznetsov,[4] V.D. Zhivulko,[7] O.M. Borodavchenko,[7] A.V. Mudryi,[7] J. Krustok[8] and R.W. Martin[1]

[1]Department of Physics, SUPA, University of Strathclyde, 107 Rottenrow, Glasgow, G4 0NG, UK
[2]M.N. Miheev Institute of Metal Physics of UB RAS, 18 S. Kovalevskaya Street, 620108, Ekaterinburg, Russia
[3]Ural Federal University, Mira 19, 620002 Ekaterinburg, Russia
[4]Institute of Solid State Chemistry of UB RAS, 91 Pervomaiskaya, 620990 Ekaterinburg, Russia
[5]Skolkovo Institute of Science and Technology, Skolkovo Innovation Center, 3 Nobelya Street, Building X, Moscow 143026, Russia
[6]Northumbria Photovoltaic Application Group, Faculty of Engineering and Environment, Northumbria University, Ellison Place, Newcastle upon Tyne NE1 8ST, UK
[7]Scientific-Practical Material Research Centre of the National Academy of Science of Belarus, P. Brovki 19, 220072 Minsk, Belarus
[8]Tallinn University of Technology, Ehitajate tee 5, 19086 Tallinn, Estonia

E-mail: michael.yakushev@strath.ac.uk

Abstract

$Cu_2ZnSnSe_4$ (CZTSe) is a semiconductor used as the absorber layer in highly promising sustainable thin film solar cells. We study the effect of Ar^+ etching of copper deficient and zinc excess CZTSe thin films deposited on Mo/glass substrates on the surface elemental composition, measured by X-Ray Photoelectron Spectroscopy (XPS), and Photoluminescence (PL) spectra. Low temperature PL spectra reveal a broad asymmetrical band at 0.95 eV. The temperature and excitation intensity dependencies of this band suggest that it is a free to bound (FB) recombination of electrons from the conduction band with holes localised at an acceptor affected by potential fluctuations. The surface composition of the as grown films demonstrates a strong copper deficiency: [Cu]/[Zn+Sn] = 0.33. Etching of the film surface using Ar^+ beam increases [Cu]/[Zn+Sn] to 0.51, which is significantly smaller than that of 0.78 in the bulk, measured by wavelength dispersive x-ray analysis, demonstrating the presence on the surface of a copper-depleted layer. The Ar^+ etching drastically reduces the FB band intensity by a factor of 4.5, broadens it and develops a low energy tail. Ar ions displace atoms in CZTSe lattice creating primary radiation defects, vacancies and interstitials, which recombine at room temperature forming antisite defects with deep energy levels. Some of them generate the observed low energy tail and increase the mean depth of potential fluctuation γ, determined from the shape of the low energy side of FB band, from 24 meV before Ar^+ etching to 35 meV after. Other deep defects work as non-radiative recombination centres reducing the intensity of the FB band.

Keywords: $Cu_2ZnSnSe_4$, argon ion etching, photoluminescence

1. Introduction

$Cu_2ZnSnSe_4$ (CZTSe), is a semiconductor compound used as the absorber layer in thin film solar cells [1]. This material is a further development of $Cu(InGa)Se_2$ (CIGS) used in solar cells which are amongst leading thin film photovoltaic (PV) devices in terms of conversion efficiencies [2]. The substitution of rare and expensive In and Ga in the CIGS chalcopyrite structure with cheap and earth-abundant Zn and Sn, alternating on the cation sub-lattice, results in a kesterite structure of CZTSe [1]. Since achieving a record conversion efficiency of 11.6% for laboratory size solar cells [3] CZTSe has become one of the most promising materials for the absorber layer in sustainable thin film PV.

A strong feature of CZTSe is the marked similarity of its structural and electronic properties with those of CIGS facilitating the use of technological solutions, once developed for CIGS-based PV devices [4,5]. However CZTSe in many aspects is very different and more complicated material [1,5]. Its electronic properties are known mostly from theoretical studies [5]. Very little information can be found in the literature on the influence of general semiconductor processing procedures like etching on the electronic properties [6,7]. CZTSe does not have such advantage of CIGS as its extremely high absorption. The CZTSe absorption coefficient of $4x10^4$ cm^{-1} [8] is rather moderate. An improvement of absorption without increasing the thickness of the absorber layer has been achieved for Si-based solar cells by anti-reflective texturing of the surface on a micrometre scale [9]. Further improvements can be achieved by the formation of a gradient in the refractive index introduced by texturing with nanoscale features [10]. Such texturing can be fabricated by dry ion-based etching which in comparison with wet etching techniques has advantages of higher resolution and etching rate as well as better reproducibility [11,12]. Also dry etching with keV ions of argon is widely used for cleaning the surface of samples for X-Ray Photoelectron Spectroscopy (XPS) [13] used to

examine surface elemental composition and electronic band structure [7,14,15]. However nothing can be found in the literature on how such a treatment influences the electronic properties of CZTSe.

Photoluminescence (PL) is one of the most sensitive techniques to study the electronic properties of semiconductors [16]. Being a non-destructive technique PL also does not require applying contacts. PL spectra can yield important information on the electronic structure and defect nature in CZTSe at a wide range of doping levels from a very low, when low temperature spectra reveal multiple emission bands and excitonic features [17], to very high, when the spectra demonstrate a broad and asymmetrical single band associated with valence band tails [18]. Particular technological interest attracts copper deficient and zinc excess CZTSe films used in high efficiency solar cells [1,5].

In this study we examine how Ar ion etching of the surface of copper deficient and zinc excess CZTSe thin films for XPS measurements influences their surface elemental composition and PL spectra.

2. Experimental details

CZTSe thin films were synthesised by the selenisation of metallic precursors deposited on Mo-coated soda-lime glass. The copper, zinc and tin precursors, prepared by magnetron sputtering of high purity elemental targets, were selenised for 5 minutes at 300 ºC and then for 15 minutes at 500 ºC. More details on the film fabrication can be found in [19,20].

The surface morphology of the as grown films was analysed by scanning electron microscopy (SEM) at electron beam energy of 5 keV. The elemental composition was measured as the average of ten measurements along a line across the surface of the films using wavelength dispersive X-ray (WDX) microanalysis at electron beam energy of 10 keV.

The structural properties of the films and the presence of secondary phases before the Ar^+ etching were examined by X-ray diffraction (XRD) measurements carried out using a Siemens D-5000 diffractometer in the Bragg–Brentano geometry and a Cu K-α radiation source (λ = 0.15406 nm).

The surface elemental composition of the as grown films and after the Ar ion etching was evaluated using a VG ESCALAB MKII X-ray electron (XPS) spectrometer. For the measurements the films were kept under a pressure of 10^{-8} Bar. The Cu, Zn, Sn and Se content of the top 6-8 atomic layers was examined by analysing Cu3*p*, Zn3*d*, Sn4*d* and Se3*d* photoelectron emission bands excited by Mg $K_{\alpha 1,2}$ - photons (1253.6 eV). The surface of the films was etched employing ESCALAB MKII ion gun with a fluence of 2×10^{16} cm^{-2} of 4 keV Ar ions directed 60º to the surface normal. This is a typical cleaning procedure to remove oxides from the surface with an Ar^+ beam of 20 μA/cm^2 [13,14].

Measurements of the PL spectra and of their temperature and excitation intensity dependences were carried out using a 1 m focal length monochromator. The 514 nm line of an Ar^+ ion laser was used for excitation of PL emission. The samples were measured at temperatures from 6 K to 300 K using a closed-cycle helium optical cryostat. The PL emission in the spectral range from 0.9 μm to 1.7 μm was detected by a cooled Hamamatsu photomultiplier tube. More experimental details on the setup for PL measurements can be found in Refs. [17,18].

Photoluminescence excitation (PLE) spectra were measured in a helium bath cryostat at 4.2 K. The PLE signal was measured at 0.95 eV near the maximum intensity of the dominant PL band using a 0.6 m focal length single grating monochromator, InGaAs photodiode sensitive in the region from 0.9 μm to 1.9 μm. A combination of a 400 W halogen tungsten lamp with 0.3 m focal length single grating monochromator was used for excitation. More experimental details can be found in Ref. [20].

Solar cells were produced by wet etching the as grown CZTSe films for 30 seconds with a 10 wt% KCN solution, deposition of CdS buffer layer, using a standard chemical bath process, and then magnetron sputtering of ZnO/ZnO:Al transparent front contacts. Solar cell parameters were measured under 100 mW/cm^2 illumination by a AM1.5 solar simulator at 25ºC using 3×3 mm^2 mechanically scribed solar cells. Principal solar cell parameters of V_{oc} = 434 mV, J_{sc} = 31.2 mA/cm^2 and FF = 59.6 resulted in a conversion efficiency of η = 8.1% [19].

3. Results

The cross section and top view SEM images of the as grown CZTSe films, shown in Fig.1(a) and (b), respectively, demonstrate a dense and homogeneous films with a thickness of 1.5 μm and a grain size in excess of 1 μm.

The WDX measurements reveal compositions of Cu: 21.8 at.%, Zn: 15.2 at.%, Sn: 12.9 at.% and Se: 50.1 at.%. These data show that the bulk ratios of metals have a copper deficiency [Cu]/[Zn+Sn] = 0.78 ± 0.10 and zinc excess [Zn]/[Sn] = 1.18 ± 0.17 whereas the ratio of Se to the sum of metals is close to the ideal stoichiometry [Se]/[Cu+Zn+Sn] = 1.00 ± 0.01 as shown in Table 1.

The near-surface elemental composition of the films was examined by XPS. XPS survey spectra before and after Ar^+ etching are shown in Fig. 2. The effect of the etching on the XPS peaks used to determine the surface elemental composition can be seen in Fig.3(a). The etching increases their yield by a factor of 5 as shown in Fig.3(a) whereas the oxygen content is reduced by a factor of 30 as it can be seen in Fig.3(b). The surface elemental composition of the as grown films (Cu: 7.0 at.%, Zn:11.8 at.%, Sn: 9.6 at.%, Se: 23.7 at.%, O: 48.0

at.%) suggests the presence of high concentrations of oxides. The XPS-measured composition after the etching was Cu: 16.6 at.%, Zn:17.9 at.%, Sn: 15.0 at.%, Se: 49.1 at.%, O: 1.5 at.%.

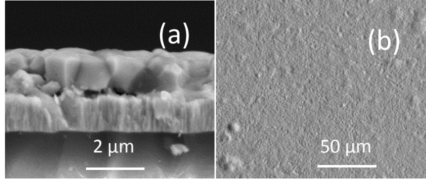

Fig.1. Cross section (a) and top view (b) SEM micrographs of the film before irradiation.

The PL spectra of the films, measured at 6 K and an excitation power density of 0.33 W/cm^2, before and after the etching, are shown in Fig.4(a).

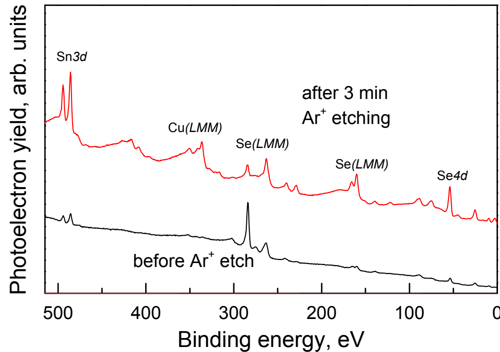

Fig.2. (Color on line) XPS survey spectra of the CZTS film before and after Ar$^+$ etching.

The oscillations near 0.9 eV are due to water vapour absorption. Both spectra are dominated by a broad and asymmetrical band with its maximum at 0.946 eV.

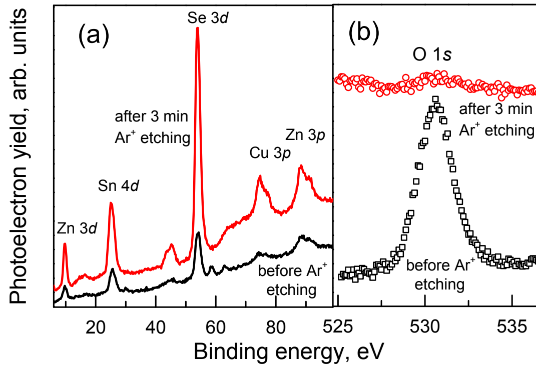

Fig.3. (Color on line) The evolution of the XPS spectrum after 3 min of 4 keV Ar$^+$ etching of the CZTSe film: Cu, Zn, Sn and Se lines (a), oxygen line (b).

Fig.4 demonstrates a drastic decrease in the intensity of this dominant band by a factor of 4.5 whereas it's full width at half maximum (FWHM) increases from 90 meV to 94 meV as shown in Table 2. The Ar$^+$ etching also makes the slope of the low energy side gentler and induces a low energy tail, which extends beyond the limit of the detector sensitivity.

The dependencies of the PL spectra on the laser excitation intensity for the film before and after the etching are shown in Fig.5. The shape of the dominant band does not depend on the excitation intensity. The PL intensity $I(P)$, calculated as the integrated intensity under the dominant band curve, depends on the excitation laser power P as $I \sim P^k$. The k power coefficient can be measured as the gradient of $I(P)$ plotted on a log-log scale as shown in Fig.5(c) and (d). The value of k close to unity, determined for the as grown film, does not change significantly after the etching. Both values are shown in Table 2.

Table 1. The [Cu]/[Zn+Sn], [Zn]/[Sn] and [Se]/[Cu+Zn+Sn] atomic ratios in the films.

Element ratios	WDX	XPS as grown	XPS After Ar$^+$ etching
[Cu]/[Zn+Sn]	0.78± 0.10	0.33± 0.02	0.51± 0.03
[Zn]/[Sn]	1.18± 0.17	1.23± 0.06	1.19± 0.06
[Se]/[Cu+Zn+Sn]	1.00± 0.01	0.83± 0.04	0.99± 0.05
[O]/[Cu+Zn+Sn+Se]	-	0.92± 0.05	0.01± 0.00

Radiative recombination of charge carriers localised at defects with energy levels within the bandgap usually results in k values smaller than unity [21,22] whereas k greater than unity is associated with excitonic-like transitions not involving defects. In the kesterites, whose PL spectra reveal a broad asymmetrical band associated with valence band tails, the closeness of k to unity has been explained by the presence in the dominant emission band of an additional unresolved band-to-band (BB) transition, recombination of free electrons from the conduction band with free holes from the valence band [23].

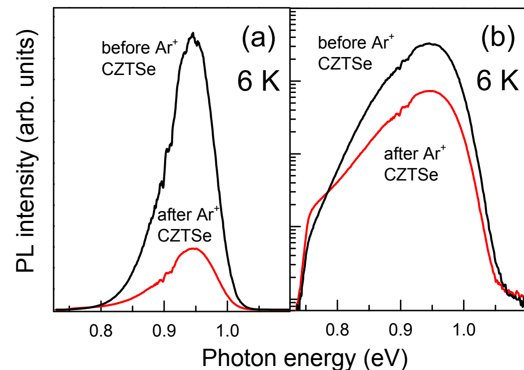

Fig.4. (Color on line) PL spectra of CZTSe/Mo films before and after etching the film with 4 keV Ar$^+$ shown on a linear (a) and logarithmic (b) scale.

Such a BB transition has been observed in CZTSe PL spectra at cryogenic temperatures [24]. In the spectra of the as grown films the increasing laser

power blue shits the dominant PL band at a rather high rate (j-shift) of 11.5 ± 0.2 meV per decade. The j-shift of this band after the etching increases to 12.6 ± 0.2 meV per decade.

Fig.6 shows the temperature dependence of the PL spectra, measured in the films before (a) and after (b) cleaning, on a logarithmic PL intensity scale. The spectra demonstrate a clear red shift of the dominant band with increasing temperature. The band gradually quenches with rising temperature. At temperatures above 150 K another broad band at about 1.05 eV becomes visible. Such a peak has been assigned to the BB recombination [20, 24]. It might also include a low intensity and high energy band with its maximum at 1.2 – 1.3 eV, which has been observed in PL spectra of CZTSe at room temperature and assigned to defects of ZnSe, a secondary phase in zinc excess CZTSe [25]. The bandgap of the CZTSe film before the etching has been determined from PLE spectra measured at 4.2 K.

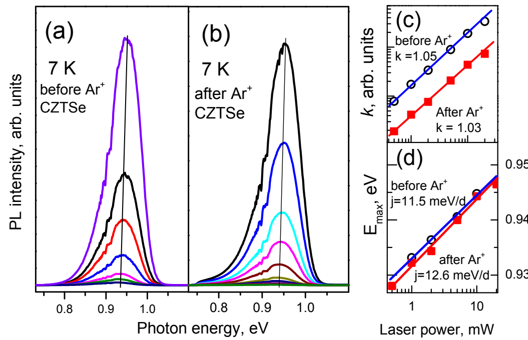

Fig.5. (Color on line) Excitation intensity dependence of PL spectra of CZTSe/Mo films before (a) and after (b) the Ar^+ surface etching, the integrated PL intensity I dependence of the band on the excitation (c) and the band maximum spectral position (d) on laser power P before (○) and after (■) etching.

The absorbance $\alpha(hv)$, where hv is photon energy, is determined from the low energy side of the PLE spectra. This side has been fitted with sigmoidal functions described in [26] as:

$$\alpha(hv) = \alpha_0/[1 + exp(E_g - hv)/\Delta E], \qquad (1)$$

where α_0 is a PLE intensity scale parameter whereas ΔE is a broadening energy depending on the gradient of the low energy side of the spectrum [27]. The best fit was achieved for E_g = (1.03 ± 0.01) eV and ΔE of 20 meV as shown in Table 2.

4. Analysis of PL spectra

Copper deficient and zinc excess CZTSe absorbers contain high concentrations of both n- and p-type defects [1,5]. These deviations from the ideal stoichiometry are necessary to achieve high performance of the solar cells with such absorbers. In the kesterites and chalcopyrites in general, and in CZTSe in particular, the effective electron mass of electrons is much lighter than that of holes. The density of state masses of electrons m^*_e and holes m^*_h in CZTSe are $0.08m_0$ and = $0.21m_0$, respectively [28].

Therefore the condition for high doping, when the defect Bohr radius exceeds the average distances between defects, can be satisfied for donors at concentrations much lower than those for acceptors. To achieve such a high doping condition in the chalcopyrites the acceptor concentration should be 22 times higher than that of donors [29]. As a result it has been assumed that the indium excess CIGS absorbers (the deviation from stoichiometry required to fabricate high performance solar cells) are degenerate in terms of donors whereas in terms of acceptors they are they behave as conventional semiconductors [30]. In the kesterites such an excess of the acceptor concentration over that of donors is 17 times, which is also very high [29], suggesting that the kesterites are likely to be highly doped in terms of donors but are conventional semiconductors in terms of acceptors.

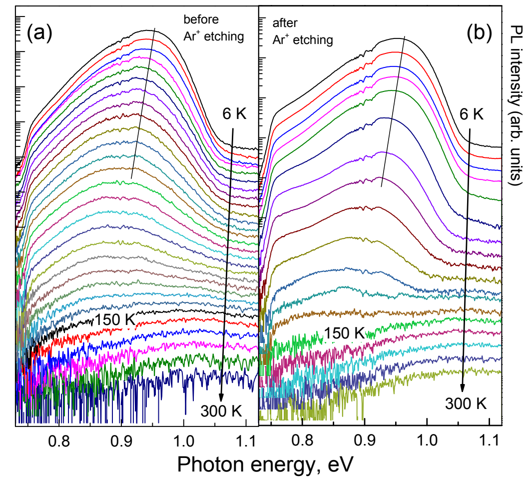

Fig.6. (Color on line) Temperature dependence of PL spectra from CZTSe/Mo film on a logarithmic scale before (a) and after (b) Ar etching. The straight lines show clear red shifts of the band maxima with increasing temperature.

According to this model low temperature PL spectra of CZTSe can have two likely bands: (1) band-to-tail (BT) transition, the recombination of holes, localised at levels in the valence band tail, and (2) free electrons at the conduction band and free-to-bound (FB) transition – the recombination of free electrons with holes captured by an acceptor. The energy level of such an acceptor should be deeper than the average depth of the valence band potential fluctuations which influence the energy level of this acceptor spreading it into a band. The characteristic features - asymmetric shape of FB, very large j-shift, reflecting the compensation level of the material [29], and a clear red shift of its maximum at increasing temperature are very similar to those of the BT bands [22,30,31]. The low-energy side of PL emission peaks carries information about the electronic properties of the semiconductor [22, 33].

For band-tail related PL bands, measured at low temperatures, the shape of the low-energy side can be used to estimate the average depth of the valence band tail [30,31].

Table 2. Spectral positions, FWHM, *j*-shifts, *k*, *γ*, and E_a of the PL band before and after the etching.

PL band parameter	Before Ar^+	After Ar^+
E_{max} (eV)	0.95	0.95
FWHM (meV)	90	93
j-shift (meV/decade)	11.5±0.2	12.6±0.2
k	1.05±0.01	1.03±0.02
γ (meV)	24±2	35±3
E_a(meV)	63±8	88±3

The shape of the dominant PL band *I(hν)*, associated with the valence band tail, can be accurately fitted with the double sigmoidal function (DSF) [30]:

$$I(h\nu) = A\left\{1+\exp\left[-\frac{(h\nu - E_1)}{W_1}\right]\right\}^{-1} * \left\{1-\left(1+\exp\left[-\frac{(h\nu - E_2)}{W_2}\right]\right)^{-1}\right\}, \quad (2)$$

where A is a PL intensity scale parameter and E_1, W_1, E_2 and W_2 are fitting parameters. W_1 and W_2 determine the slopes of the low and high energy sides, respectively, and the fitted W_1 can be used as an estimate of the average depth of the valence band tail *γ*. Fig.7 shows best fits of the DSF to PL bands, measured at 6 K, before and after the Ar^+ etching. The figure shows that the fitted functions reproduce well the low energy side of the band. Values of *γ* of 24 and 35 meV, determined from the spectra before and after etching, respectively, are shown in Table 2.

To identify which type of transition BT or FB we observe in our spectra we compare *γ* with the activation energy E_a of the temperature quenching of the dominant band determined using Arrhenius analysis. If E_a is smaller than *γ* then the band can be assigned to BT alternatively the band is likely to have the FB nature [20,22,31].

The use of DSF significantly improves the accuracy of the temperature dependence analysis of the dominant band because it provides an opportunity to subtract the BB band. Although the BB band is present in the PL spectra measured at all temperatures at low temperatures its intensity I_{BB} is much smaller than that of the dominant band I_D. At 6 K the I_D/I_{BB} ratio is of 440, so we can neglect its contribution whereas at 130 K I_D/I_{BB} becomes close to unity and neglecting its contribution would result in a significant error of E_a. Arrhenius plots of the integrated intensities *I(T)* for the dominant band before and after the etching are shown in Fig. 8. To determine E_a these plots were fitted by the following expression assuming a temperature-dependent hole capture cross section [34]:

$$I(T)=I_0 / [1+A_1T^{3/2}+A_2T^{3/2}\exp(-E_a/k_BT)], \quad (3)$$

where I_0 is the intensity of the band at 6 K, whereas A_1 and A_2 are rate parameters.

The determined E_a before and after the etching, 63 ± 8 meV and 88 ± 3 meV, respectively (also shown in Table 2) are greater than *γ* suggesting that the dominant band in both spectra are FB-related and involve recombination of free electrons with holes localised at conventional acceptors with their energy levels spread by spatial potential fluctuations.

The temperature dependencies of the dominant band before and after the etching, shown in Fig.6, demonstrate clear red shifts with rising temperature. At low temperatures holes are localised at valence band tail states, acting like hydrogenic acceptors. Unlike conventional acceptor levels these acceptor-like states are energetically spread by the potential fluctuation increasing the width of the PL band formed by the recombination of free electrons and holes, localised at these tail states.

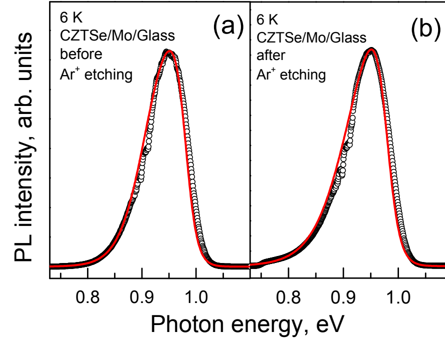

Fig.7. (Color on line) Double sigmoidal functions (solid line) fitted into the PL spectra (○) of CZTSe/Mo/Glass (measured at 6 K) before (a) and after Ar^+ etching (b).

In turn the FB recombination includes recombination of free holes, first captured at the acceptor, and holes from the valence band tail states. Therefore the FB band behaves on rising temperature similar to BT. The valence band tail also determines the shape of the low energy side of FB [22,29,30]. Increasing temperature thermalises the holes at shallower states of the acceptor-like states of the valence band tail into the valence band whereas holes at deeper states remain localised. These processes red shift the maximum of the BT and FB bands. The holes thermalised to the valence band can recombine with free electrons. Such a recombination can be seen in the PL spectra as the BB band.

5. Discussion

The XPS measured elemental ratios of the surface of the as-grown film, demonstrate a strong copper deficiency [Cu]/[Zn+Sn] = 0.33±0.02, which is much more significant than the 0.78±0.10 in deeper layers of the film measured by WDX as shown in Table 1. The XPS-measured [Zn]/[Sn] = 1.23 ± 0.06 is within the error range of [Zn]/[Sn] = 1.18 ± 0.17 for the bulk whereas the XPS measured [Se]/[Cu+Zn+Sn] = 0.83 ± 0.04 demonstrates a

selenium deficiency unlike a near stoichiometric selenium content of 1.00 ± 0.01 measured by WDX. The upper layer in the as grown films contains a significant concentration of oxygen [O]/[Cu+Zn+Sn+Se] = 0.92 ± 0.06.

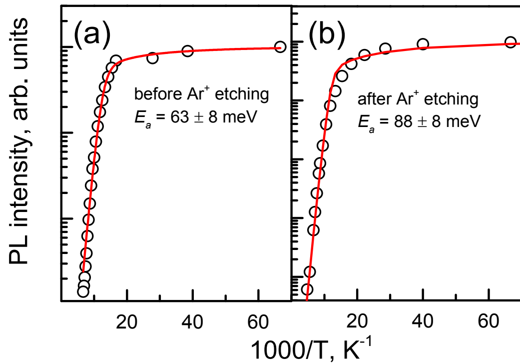

Fig.8. (Color on line) Arrhenius plots of the dominant band integrated intensities for CZTSe/Mo/Glass before (a) and after (b) Ar^+ etching.

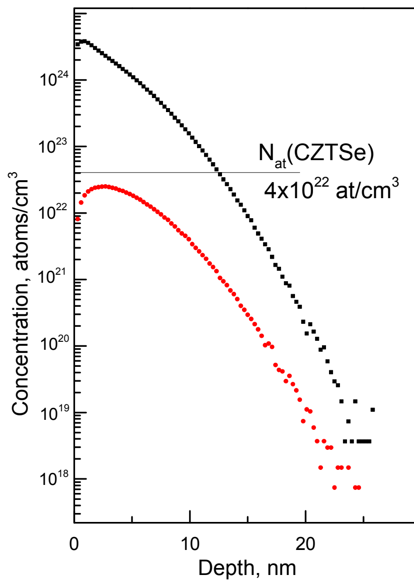

Fig.9. (Color on line) TRIM code simulation of the depth distribution of Ar^+ (●), implanted in CZTSe with a fluence of 2×10^{16} cm^{-2} and energy 4 keV, and vacancies (■) generated by this implantation. The straight line shows the CZTSe atomic density.

After the etching the surface becomes less copper deficient [Cu]/[Zn+Sn] = 0.51±0.03, although this deficiency is still significantly greater than that in the bulk suggesting the presence at the surface of a copper depleted layer. The formation of a copper deficient layer has been reported at the surface of $CuInSe_2$ and CIGS [35,36]. It was attributed to the reconstruction of polar surfaces under the influence of surface charges [37]. A similar copper depletion was reported for $Cu_2ZnSn(SSe)_4$ mono-grain powder [13]. Both the zinc excess [Zn]/[Sn] = 1.19±0.06 and the near stoichiometric Se content [Se]/[Cu+Zn+Sn] = 0.99±0.05 become very close to their bulk values after the etching.

Accelerated ions of Ar penetrate into the near surface layer of the CZTSe lattice. A TRIM [38] calculated depth distribution of 4 keV Ar, implanted in CZTSe with a dose of 2×10^{16} cm^{-2}, is shown in Fig.9. The theoretical concentration of argon at its maximum reaches a half of the atomic density in CZTSe, $N_{at} = 4.3\times10^{22}$ at/cm^3, calculated assuming a density of 5.62 g/cm [39]. Although the calculations indicate that more than 85% of Ar ions are distributed in the first 10 nm of CZTSe quite a high concentration of argon can be found in deeper layers: concentrations in excess of 10^{20} at/cm^3 can be found at up to 20 nm whereas in a layer at 25 nm the concentration of argon can be above 10^{18} at/cm^3. The calculations however do not take in account the effect of sputtering of the Cu, Zn, Sn and Se atoms from the surface by argon ions. Sputtering gradually removes the upper atomic layers of CZTSe, filled with argon atoms implanted into the layer previously and prevents its accumulation. That is why the dose of implanted ions of Ar is expected to be lower than the fluence of 2×10^{16} cm^{-2}. Embedded atoms of Ar may stay in the lattice as interstitials distorting it. Also they might accumulate in microbubbles causing the formation of extended defects and blistering of the surface. Extended defects (dislocations and stacking faults) [40], micro-bubbles along with blistering effects [41] were observed in single crystals of $CuInSe_2$, bombarded with keV ions of Xe^+.

Energetic ions of Ar collide with atoms of the CZTSe lattice and displace them forming primary structural defects, vacancies and interstitial atoms of Cu, Zn, Sn and Se. The displaced interstitial atoms can also displace more atoms from the lattice sites in collision cascades. A theoretical distribution of primary defects caused by a 2×10^{16} cm^{-2} dose of Ar^+ is shown in Fig.9. According to TRIM code simulations about 97% of the primary defects are accumulated in the first 8 nm layer of CZTSe. The theoretical concentration maximum of such defects exceeds the atomic density of CZTSe by about two orders of magnitude whereas significant concentrations of vacancies (in excess of 10^{18} per cm^3) can be found to a depth of 25 nm.

At room temperature primary structural defects in semiconductors are known to be unstable. They interact with each other as well as with the surrounding crystalline lattice forming more stable secondary defects and defect complexes. The formation of secondary defects during and shortly after the etching of semiconductors with heavy ions is enhanced by “thermal spikes” [42], micro-volumes surrounding collision cascades with the majority of atoms in motion. Such motion can be interpreted in terms of an increase of the local temperature. Theoretical estimates of the spike temperature, generated by 30keV Ar^+, propagating in $CuInSe_2$ predict an increase in the temperatures up to 1700 K during 10^{-11} s [43]. Such temperatures facilitate an effective healing of the $CuInSe_2$ structure and the formation of extended defects. The

healing and defect formation processes were observed in $CuInSe_2$ single crystals by transmission electron microscopy *in-situ* with irradiation by keV ions of Xe^+ [44]. The chalcopyrite structure of $CuInSe_2$ with ordered Cu and In atoms on the cation sub-lattice, was reported to transform to a sphalerite one with randomised positions of Cu and In [45] under 1.5 keV Ar^+ bombardment. Such a randomisation can be represented as a high concentration of the antisite defects copper-on-indium site Cu_{In} and indium-on-copper site In_{Cu}.
Assuming similarities of the structural and electronic properties of CZTSe and $CuInSe_2$ we can expect primary defects of CZTSe, created by argon ions, to be quickly healed during and shortly after the etching by the recombination of vacancies with interstitials. In particular we can expect high concentrations of Zn_{Cu} due to zinc excess and copper deficiency. Also we can expect the formation of the donors Cu_{Zn}, whose formation energy in CZTSe is very low [5], and their neutral defect complexes with the acceptor V_{Cu}: Cu_{Zn}+V_{Cu}. High concentrations of primary and antisite defects, donors as well as acceptors with greater formation energies can also be present in the damaged layer. According to theoretical calculations [5] energy levels of antisite defects are mostly rather deep. In the kesterites the formation of acceptor-type of defects reduces the formation energy of donors which should increase the compensation level in the damaged layer. Such an increase in the compensation level is reflected by the *j*-shit increase. Some of the secondary defects can generate deep radiative emission bands whereas others can act as deep non-radiative traps of charge carriers. In GaAs the band tail depth has been found to be determined by the compensation level [32]. This is consistent with the observed increase in γ from 24 meV before to 35 meV after the Ar^+ etching. Antisite defects in CZTSe are thought to be responsible for the band tails [46]. The presence of defects with deep PL emission bands is consistent with the observed low energy tail of FB whereas high concentrations of non-radiative recombination centres can be responsible for the observed reduction of the intensity of the FB band. The increase of the activation energy of an acceptor, associated with the FB band, from 63 meV to 88 meV is also consistent with new deep acceptors generated by the Ar^+ etching. Deep non-radiative defects are expected to act as traps of charge carriers reducing their concentration and mobility whereas the resistivity of the films after the Ar^+ etching should increase.

Assuming the absorption coefficient of CZTSe to be of 3.5×10^4 cm^{-1} [8] at 2.4 eV we can estimate the thickness of the layer excited by 514 nm photons as 300 nm. This is an order of magnitude thicker than the damaged layer. It means that the observed PL spectrum, measured after the Ar^+ etching, is likely to be a combination of PL from the thin upper layer damaged by Ar^+, represented by the low energy tail, and PL from a thicker undamaged layer generating the FB band we observed before irradiation.

4. Conclusion

Effects of a 4 keV Ar^+ surface etching on PL and XPS spectra of CZTSe/Mo/glass (used to fabricated solar cells achieving efficiencies of 8.1%) are studied. The PL spectra, measured at 6 K, before and after the etching, reveal a broad asymmetrical band at 0.95 eV, identified as the FB transition, involving recombination of free electrons from the conduction band with holes localised at an acceptor affected by valence band potential fluctuations. The XPS spectra of the as-deposited films demonstrate a strong copper deficiency [Cu]/[Zn+Sn] = 0.33. Etching by Ar^+ increases [Cu]/[Zn+Sn] to 0.51, which is much smaller than the bulk value of 0.78, suggesting the formation of a Cu-depleted surface layer. After the etching the intensity of the PL band falls by a factor of 4.5. It becomes broader and develops a strong low energy tail. Ar^+ displace atoms in the CZTSe lattice creating primary radiation defects, vacancies and interstitials, which recombine at room temperature during and shortly after the etching. They form deep antisite defects, donors and acceptors, generating the observed low energy tail and increasing the mean depth of potential fluctuation from 24 meV before to 35 meV after the Ar^+ etching. They also form non-radiative recombination centres reducing the intensity of the PL by a factor of 4.5. The observed PL spectra combine emission from the damaged layer, represented by the low energy tail, and the FB band from the deeper undamaged CZTSe.

Acknowledgments

This study was supported by the Russian Science Foundation (project No 17-12-01500). PLE measurements were supported by grant BRFFR F18M-042. The interpretation of the experiments was partly supported by institutional research funding IUT (IUT19-28) of the Estonian Ministry of Education and EU Regional Development Fund (project TK141).

References

[1] S. Siebentritt, S. Schorr, Prog Photovolt.: Res. Appl. **20**, 512 (2012).
[2] P. Jackson, R. Wuerz, D. Hariskos, E. Lotter, W. Witte, M. Powalla, Phys. Status Solidi R **10,** 583 (2016).
[3] Y.S. Lee, T. Gershon, O. Gunawan, T.K. Todorov, T. Gokmen, Y. Virgus, S. Guha, Adv. Energy Mater. **12**, 1401372 (2015).
[4] M.J. Romero, H. Du, G. Teeter, Y. Yan, M.M. Al-Jassim, Phys. Rev. B **84**, 165324 (2011).
[5] S. Chen, A. Walsh, X.G. Gong, S.H. Wei, Adv. Mater. **25**, 1522 (2013).
[6] M. Buffière, G. Brammertz, S. Sahayaraj, M. Batuk, S. Khelifi, D. Mangin, A. El Mel, L. Arzel, J.

Hadermann, M. Meuris, and J. Poortmans, ACS Appl. Mater. Interfaces **7**, 14690 (2015).
[7] M. Bar, B.-A. Schubert, B. Marsen, S. Schorr, R. G. Wilks, L. Weinhardt, S. Pookpanratana, M. Blum, S. Krause, Y. Zhang, W. Yang, T. Unold, C. Heske, and H.-W. Schock, Phys. Rev. B, **84,** 035308 (2011).
[8] M.I. Amal, K.H. Kim, Chalcogenide Lett. **9**, 345 (2012).
[9] D.H. Macdonald, A. Cuevas, M.J. Kerr, C. Samundsett, D. Ruby, S. Winderbaum, and A. Leo Sol. Energy **76**, 277 (2004).
[10] P. Lalanne and G.M. Morris Nanotechnology **8**, 53 (1997).
[11] P.J. Kelly, R.D. Arnell, Vacuum **56**, 159 (2000).
[12] J. Yoo, Reactive ion etching (RIE) technique for application in crystalline silicon solar cells, Solar Energy **84**, 730 (2010).
[13] C.D. Wagner, W.M. Riggs, L.F. Davis, J.F. Moulder, G.E. Mullenberg, *Handbook of X-ray Photoelectron Spectroscopy* (Perkin-Elmer Corporation, Physical Electronics Division, Eden Prairie, Minnesota, 1979).
[14] M. Danilson, M. Altosaar, M. Kauk, A. Katerski, J. Krustok, J. Raudoja, Thin Solid Films **519**, 7407 (2011).
[15] P.-Yu Lee, S.-Po Chang, En-Hao Hsu, Sh.-J. Chang, Solar Energy Materials & Solar Cells, **128**, 156 (2014).
[16] H.B. Bebb, E. Williams, *Semiconductors and Semimetals 8* (Academic Press, New York, 1972).
[17] F. Luckert, D.I. Hamilton, M.V. Yakushev, N.S. Beattie, G. Zoppi, M. Moynihan, I. Forbes, A.V. Karotki, A.V. Mudryi, M. Grossberg, J. Krustok, R.W. Martin, Appl. Phys. Lett. **99**, 062104 (2011).
[18] M.V. Yakushev, I. Forbes, A.V. Mudryi, M. Grossberg, J. Krustok, N.S. Beattie, M. Moynihan, A. Rockett, R.W. Martin, Thin Solid Films **582**, 154 (2015).
[19] J. Márquez, M. Neuschitzer, M. Dimitrievska, R. Gunder, S. Haass, M. Werner, Y.E. Romanyuk, S. Schorr, N.M. Pearsall, I. Forbes, Sol. Energy Mater. Sol. Cells **144**, 579 (2016).
[20] M.V. Yakushev, M.A. Sulimov, J. Márquez-Prieto, I. Forbes, J. Krustok, P.R. Edwards, V.D. Zhivulko, O.M. Borodavchenko, A.V. Mudryi, R.W. Martin, Sol. Energy Mater. Sol. Cells **168**, 69 (2017).
[21] T. Schmidt, K. Lischka, W. Zulehner, Phys. Rev. B **45**, 8989 (1992).
[22] A.P. Levanyuk, V.V. Osipov, Sov. Phys. Usp. **24**, 187 (1981).
[23] J. Márquez-Prieto, M.V. Yakushev, I. Forbes, J. Krustok, V.D. Zhivulko, P.R. Edwards, M. Dimitrievska, V. Izquerdo-Roca, N.M. Pearsall, A.V. Mudryi, R.W. Martin, Sol. Energy Mater. Sol. Cells **152**, 42 (2016).
[24] M.V. Yakushev, J. Márquez-Prieto, I. Forbes, P.R. Edwards, V.D. Zhivulko, A.V. Mudryi, J. Krustok, R.W. Martin, J. Phys. D: Appl. Phys. **48**, 475109 (2015).
[25] R. Djemour, M. Mousel, A. Redinger, L. Gütay, A. Crossay, D. Colombara, P.J. Dale, S. Siebentritt, Appl. Phys. Lett. **102**, 222108 (2013).
[26] K.P. O'Donnell, *R.W. Martin,* P.G. Middleton, Phys. Rev. Lett. **82**, 237 (1999).
[27] M.E. White, K.P. O'Donnell, R.W. Martin, S. Pereira, C.J. Deatcher, I.M. Watson, Mater. Sci. Eng. B **93**, 147 (2002).
[28] C. Persson, J. Appl. Phys. **107**, 053710 (2010).
[29] J.P. Teixeira, R.A. Sousa, M.G. Sousa, A.F. da Cunha, P.A. Fernandes, P.M.P. Salomé, J.P. Leitão, Phys. Rev. B 90, 235202 (2014).
[30] J. Krustok, H. Collan, M. Yakushev, K. Hjelt, Phys. Scr. T **79**, 179 (1999).
[31] A. Jagomagi, J. Krustok, J. Raudoja, M. Grossberg, M. Danilson, M. Yakushev, Physica B **337**, 369 (2003).
[32] Z.I. Alferov, V.M. Andreev, D.Z. Garbuzov, M.K. Trukan, Radiative recombination in epitaxial compensated gallium-arsenide, Sov. Phys. Semicond. **6**, 1718 (1973).
[33] R. Bhattacharya, B. Pal, B. Bansal, Appl. Phys. Lett. **100**, 222103 (2012).
[34] J. Krustok, H. Collan, K. Hjelt, J. Appl. Phys. **81**, 1442 (1997).
[35] D. Schmid, M. Ruckh, F. Grundwald, H.W. Schock, J. Appl. Phys.**73**, 2902 (1993).
[36] M.V. Kuznetsov, E.V. Shalaeva, M.V. Yakushev, R.D. Tomlinson, Surface Science **530**, L297 (2003).
[37] S.B. Zhang, S.-H. Wei, Phys. Rev. B **65**, 081402 (2002).
[38] J.P. Biersack, L.G. Haggmark, Nucl. Instr. Meth. **174**, 257 (1980).
[39] L. Guen, W.S. Glaunsinger, J. Solid State Chem. **35**, 10 (1980).
[40] C.A Mullan, C.J Kiely, M.V Yakushev, M. Imanieh, R.D Tomlinson, A. Rockett, Phil. Mag. A **73**, 1131 (1996).
[41] A. Zegadi, A. Belattar, C.A. Faunce, E. Ahmed, S. Anwar, M.V. Yakushev, M. Imanieh, M.A. Slifkin, A.E. Hill, R.D. Tomlinson, Nucl. Instr. Meth. Phys. Res. Sect. B **94**, 429 (1994).
[42] P. Sigmund, Energy density and time constant of heavy-ion-induced elastic-collision spikes in solids, Appl. Phys. Lett. 25, 169 (1974).
[43] M.V. Yakushev, V.A. Volkov, N.N. Mursakulov, C.E. Sabzaliyeva, R.W. Martin, J. Vac. Sci. Technol. A **34**, 051203 (2016).
[44] S.E. Donnelly, J.A. Hinks, P.D. Edmondson, R.D. Pilkington, M. Yakushev, R.C. Birtcher, Nucl. Instr. Meth. Phys. Res. Sect. B **242**, 686 (2006).
[45] P. Corvini, A. Kahn, S. Wagner, Appl. Phys. **57**, 2967 (1985).
[46] T. Gokmen, O. Ganawan, T.K. Todorov, D.B. Mitzi, Appl. Phys. Lett. **103**, 103506 (2013).

DOI: 10.1021/acsam

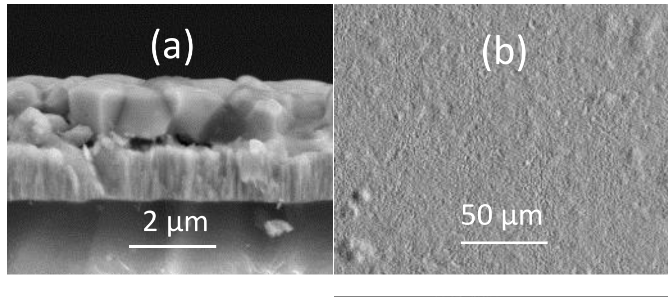
(a)
2 µm
(b)
50 µm

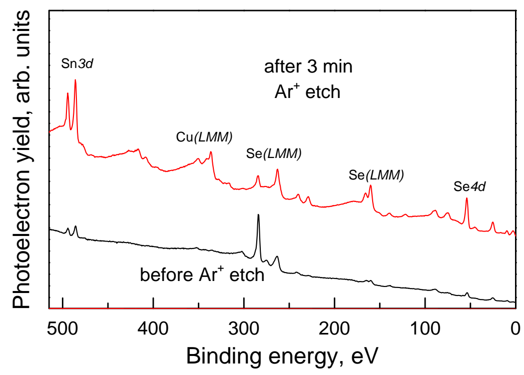
Photoelectron yield, arb. units
Sn3d
after 3 min
Ar+ etch
Cu(LMM)
Se(LMM)
Se(LMM)
Se4d
before Ar+ etch
500
400
300
200
100
0
Binding energy, eV

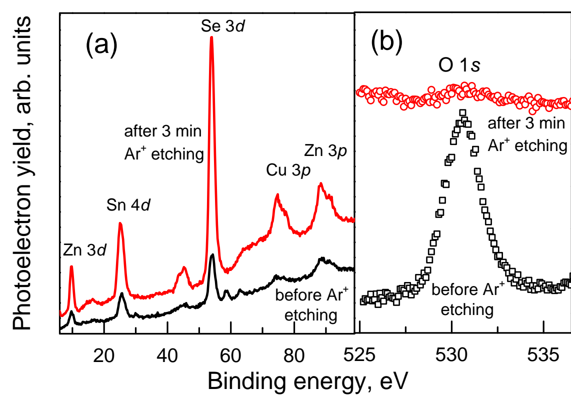
(a)
(b)
Se 3d
O 1s
after 3 min
Ar+ etching
Sn 4d
Zn 3d
Cu 3p
Zn 3p
before Ar+
etching
Photoelectron yield, arb. units
Binding energy, eV
20
40
60
80
525
530
535

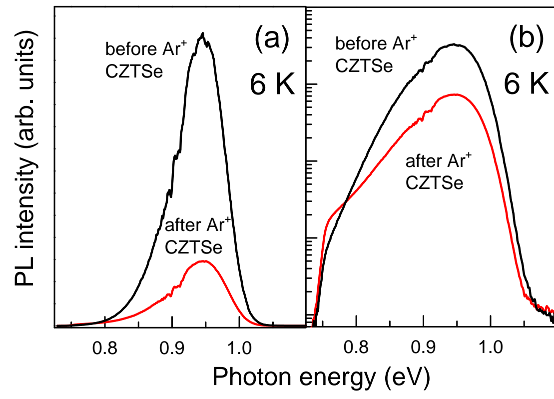

PL intensity (arb. units)
before Ar+
CZTSe
(a)
6 K
after Ar+
CZTSe
0.8
0.9
1.0
(b)
before Ar+
CZTSe
6 K
after Ar+
CZTSe
0.8
0.9
1.0
Photon energy (eV)

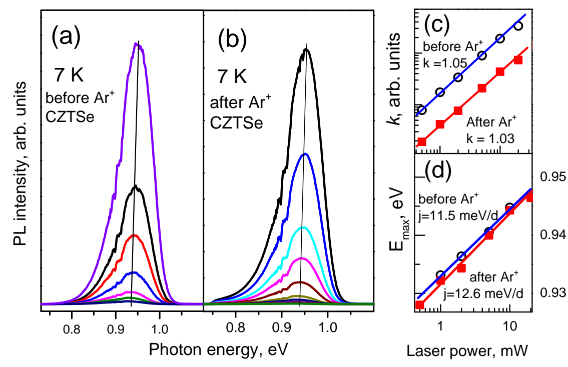

(a)
7 K
before Ar+
CZTSe
(b)
7 K
after Ar+
CZTSe
PL intensity, arb. units
Photon energy, eV
0.8
0.9
1.0
(c)
before Ar+
k =1.05
After Ar+
k = 1.03
k, arb. units
(d)
before Ar+
j=11.5 meV/d
after Ar+
j=12.6 meV/d
E_max, eV
0.95
0.94
0.93
1
10
Laser power, mW

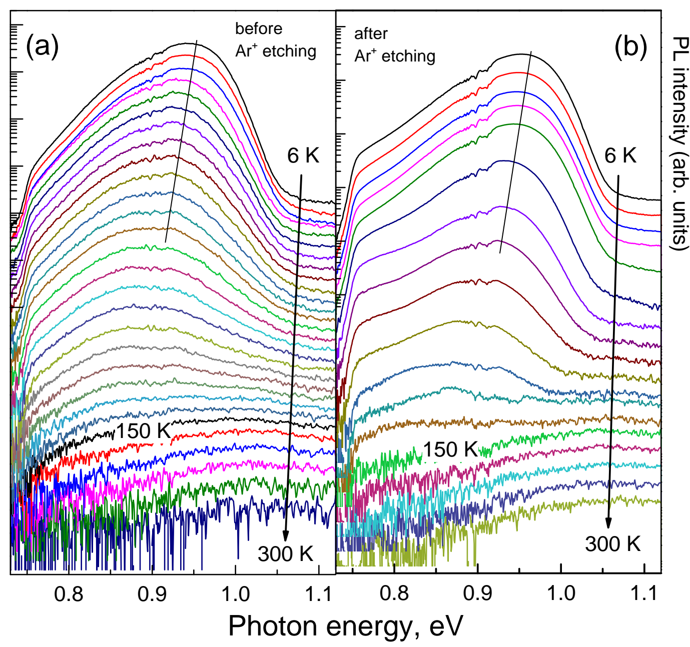

(a)
before
Ar+ etching
6 K
150 K
300 K
(b)
after
Ar+ etching
6 K
150 K
300 K
0.8
0.9
1.0
1.1
Photon energy, eV
PL intensity (arb. units)

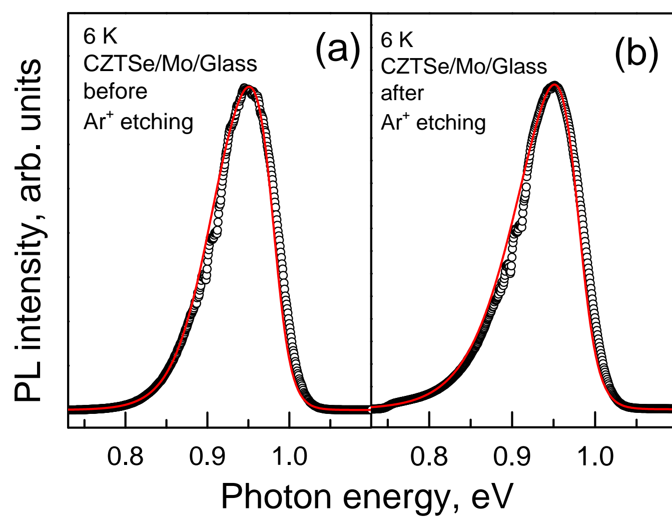
6 K
CZTSe/Mo/Glass
before
Ar+ etching
(a)
6 K
CZTSe/Mo/Glass
after
Ar+ etching
(b)
PL intensity, arb. units
0.8
0.9
1.0
0.8
0.9
1.0
Photon energy, eV

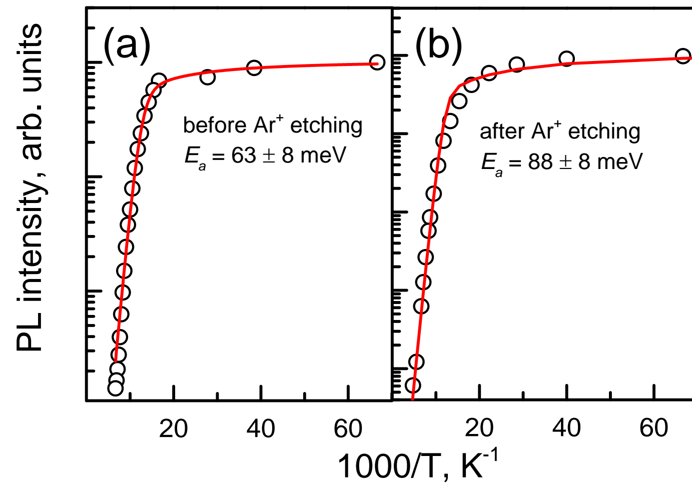
(a)
before Ar+ etching
E_a = 63 ± 8 meV
(b)
after Ar+ etching
E_a = 88 ± 8 meV
PL intensity, arb. units
20
40
60
20
40
60
1000/T, K-1

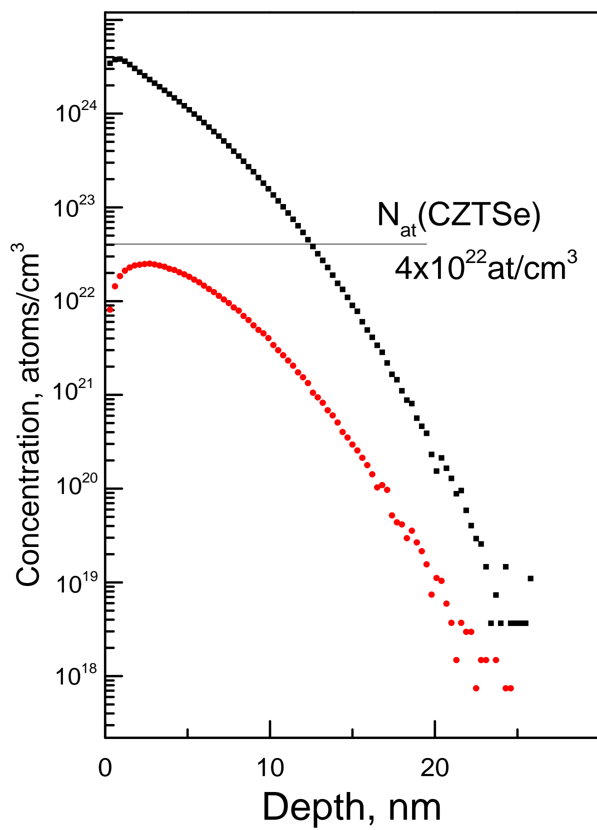

Concentration, atoms/cm^3
Depth, nm
N_at(CZTSe)
4x10^22 at/cm^3
10^24
10^23
10^22
10^21
10^20
10^19
10^18
0
10
20